Oil volume fraction and velocity profiles in vertical, bubbly oil-in-water flows

G.P. Lucas [*1] **and N. Panagiotopoulos** [2]

[1] *School of Computing and Engineering University of Huddersfield, Queensgate, Huddersfield, HD1 3DH, UK.*

[2] *European Space Research and Technology Centre, Noordwijk, Netherlands.*

[*] *Corresponding author: Tel +44 1484-472266. Email:g.lucas@hud.ac.uk*

Abstract

A series of experiments was carried out using a dual sensor conductance probe to measure the local axial oil velocity distribution and the local oil volume fraction distribution in vertical, oil in water bubbly flows in an 80mm diameter vertical pipe. Values of the water superficial velocity were in the range $0.276\,\mathrm{ms}^{-1}$ to $0.417\,\mathrm{ms}^{-1}$, values of the oil superficial velocity were in the range $0.025\,\mathrm{ms}^{-1}$ to $0.083\,\mathrm{ms}^{-1}$ and values of the mean oil volume fraction were in the range 0.047 to 0.205. For all of the flow conditions investigated it was found that the axial velocity profile of the oil droplets had a 'power law' shape which was very similar to the shape of the air velocity distributions previously observed for air-water bubbly flows at similar flow conditions. It was also found that the shape of the local oil volume fraction distribution was highly dependent upon the value of the mean oil volume fraction. For values of the mean oil volume fraction $\overline{\beta}_{ref}$ less than about 0.08, the local oil volume fraction distribution had a power law shape. For values of $\overline{\beta}_{ref}$ between about 0.08 and 0.15 the local oil volume fraction distribution was essentially flat, apart from within a bubble sub-layer close to the pipe wall. For values of $\overline{\beta}_{ref}$ greater than about 0.15 the local oil volume fraction distribution had an 'intermediate peak' shape. Mathematical modelling showed that the shapes of the observed local oil fraction distributions were a result of diffusion and of hydrodynamic forces acting upon the oil droplets. For $\overline{\beta}_{ref} < 0.08$ the net hydrodynamic force on the droplets was towards the pipe centre whilst for $\overline{\beta}_{ref} > 0.15$ the net hydrodynamic force on the droplets was biased towards the pipe wall. The nature, and relative strength, of each of the hydrodynamic forces acting on the oil droplets is discussed.

Key words: multiphase flow; conductance probe; modelling volume fraction profiles;

Nomenclature

C_0	distribution parameter
c_1	constant used in equation 14 (m)
D	internal pipe diameter (m)
f	friction factor
F	frictional pressure loss ($\mathrm{kgm^{-1}s^{-2}}$)
g	acceleration of gravity ($\mathrm{ms^{-2}}$)
h	pressure tapping separation (m)
j_l	local homogeneous velocity ($\mathrm{ms^{-1}}$)
K_0	constant used in equation 12 ($\mathrm{m^2s^{-1}}$)
K_{hy}	constant first used in equation 17 ($\mathrm{ms^{-1}}$)
K_ε	constant first used in equation 18 ($\mathrm{m^3s^{-1}}$)
n	exponent used in equation 7
N	number of droplets
p	power law exponent for velocity profile
q	power law exponent for volume fraction profile
r	radial position (m)
R	internal pipe radius (m)
t_{1f} t_{2f} t_{1r} t_{2r}	times when droplet surface contacts sensors (s)
T	sampling period (s)
u_z, u_θ, u_r	local axial, azimuthal and radial droplet velocity components ($\mathrm{ms^{-1}}$)
$\overline{u}_d$	mean dispersed phase velocity ($\mathrm{ms^{-1}}$)
U_h	homogeneous velocity ($\mathrm{ms^{-1}}$)
u_{hy}	local radial droplet velocity due to hydrodynamic forces ($\mathrm{ms^{-1}}$)
u_L	local axial velocity of continuous liquid ($\mathrm{ms^{-1}}$)
u_o	local oil velocity ($\mathrm{ms^{-1}}$)
$u_{o,\max}$	maximum local oil velocity ($\mathrm{ms^{-1}}$)
U_{os}	oil superficial velocity ($\mathrm{ms^{-1}}$)
u_{slip}	slip velocity ($\mathrm{ms^{-1}}$)
u_{t0}	single droplet terminal velocity ($\mathrm{ms^{-1}}$)
u_w	local water velocity ($\mathrm{ms^{-1}}$)
U_{ws}	water superficial velocity ($\mathrm{ms^{-1}}$)
z	axial coordinate (m)

$\overline{\alpha}$	mean air volume fraction
$\overline{\alpha}_d$	mean dispersed phase volume fraction
α_l	local dispersed phase volume fraction
β	local oil volume fraction
$\beta_{\max}$	maximum local oil volume fraction
$\overline{\beta}_{ref}$	reference measurement of mean oil volume fraction
$\delta t_{1,i}$	time interval defined in equation 1 (s)
$\delta t_{2,i}$	time interval defined in equation 2 (s)
Δp	differential pressure ($\mathrm{kgm^{-1}s^{-2}}$)
ε	diffusivity ($\mathrm{m^2 s^{-1}}$)
ρ_o	oil density ($\mathrm{kgm^{-3}}$)
ρ_w	water density ($\mathrm{kgm^{-3}}$)
θ	azimuthal coordinate (radians)

1. Introduction

This paper describes the use of a local, miniature, intrusive dual-sensor conductance probe to determine the local oil volume fraction distribution and the local oil axial velocity distribution in a range of vertical upward oil-in-water flows in the bubbly flow regime. The main objectives for carrying out the work described in this paper were: (i) to provide data for quantitative comparison with, and validation of, volume fraction and velocity profiles obtained using dual-plane Electrical Resistance Tomography (ERT) techniques [1]: (ii) to compare the local oil volume fraction and local oil axial velocity profiles with profiles obtained by the same authors in vertical, air-in-water bubbly flows [2] using a similar pipe diameter (80mm i.d.), similar phase superficial velocities, similar values for the mean dispersed phase volume fraction and similar size particles of the dispersed phase: (iii) to investigate whether the local oil volume fraction and axial velocity distributions could be represented by 'power law' approximations as has found to be the case, under certain flow conditions, for the local gas volume fraction and axial velocity distributions in vertical air-in-water bubbly flows [2], [3]: (iv) to determine values for the Zuber-Findlay [4] distribution parameter C_0 for oil-in-water flows: and (v) to attempt to provide a physical explanation for the shapes of the local oil volume fraction distributions in vertical bubbly oil-in-water flows.

The measurement of velocity and volume fraction profiles of the dispersed phase has received much less attention in the literature for oil-water flows than in is the case for gas-liquid flows. However the principal previous work in this field includes that which has been carried out by; (i) Vigneaux et al [5] who measured local oil volume fraction distributions, in vertical and inclined oil water flows in a 200mm diameter pipe, using a high frequency impedance probe; (ii) Bruun's group [6] and [7] who investigated optical and hot-wire probes as a means of measuring the local properties of vertical oil-water flows; (iii) Zhao et al [8] who measured local oil volume fraction profiles, interfacial velocity profiles, interfacial area concentration profiles and oil drop diameters in a vertical 40mm diameter tube using a double-sensor conductivity probe; and (iv) Lum et al [9] who used high speed video filming and impedance probes to measure phase distributions in oil-water flows inclined at small angles (less than 10^o) to the horizontal in a 38mm diameter pipe.

More recently, Wang et al [10] have attempted to use dual-plane ERT to measure local oil volume fraction and velocity profiles in vertical oil-in-water flows in an 80mm diameter pipe. One of the main aims of the current paper is to provide reference data against which Wang's ERT results can be compared.

2. Experimental Apparatus

2.1 The dual-sensor probe

The design and construction of the local dual-sensor conductance probe used in the present investigation, the associated electronic circuitry and the relevant signal processing techniques are all described in great detail in a previous paper [2]. However, for the benefit of the reader, a brief description of the probe and the signal processing technique is repeated here.

The probe was manufactured from two stainless steel needles which were 0.3mm in diameter and which were mounted inside a stainless steel tube of outer diameter of 4mm

(figure 1). Each needle was coated with waterproof paint and insulating varnish, which were removed from the very tip of the needle. Thus, the front and rear sensors of the probe were located at the very tips of the needles. For the probes used in the experiments described in this paper the axial sensor separation s was typically 2.5mm whilst the lateral sensor separation was typically 1mm. The 4mm stainless steel tube forming the probe body was used as a common earth electrode for both sensors. The fluid conductance at each sensor was obtained using a simple dc amplifier circuit, which measured the conductance between the tip of the relevant needle and the probe body.

Consider the situation where the two sensors of the probe are separated by an axial distance s in a vertical upward, bubbly, oil-in-water flow in which the oil droplets travel in the axial direction. Let us assume that the surface of a bubble makes first contact with the upstream (front) sensor at time t_{1f}. At this time the measured conductance at the front sensor will fall sharply. Let us further assume that the front sensor makes last contact with the surface of the droplet at time t_{2f} (this is the time at which the droplet leaves the front sensor). At time t_{2f} the measured conductance at the front sensor will rise sharply as the sensor is again surrounded by water. The times at which the rear sensor makes first and last contact with the surface of the droplet are t_{1r} and t_{2r}. Suppose N droplets hit both the front and rear sensors during a sampling period T. For the i^{th} droplet two time intervals $\delta t_{1,i}$ and $\delta t_{2,i}$ may be defined as follows

$$\delta t_{1,i} = t_{1r,i} - t_{1f,i} \qquad (1)$$

and

$$\delta t_{2,i} = t_{2r,i} - t_{2f,i} \qquad (2)$$

The mean local axial oil droplet velocity u_o at the position of the probe is then given by

$$u_o = \frac{2s}{N} \sum_{i=1}^{N} \frac{1}{(\delta t_{1,i} + \delta t_{2,i})} \qquad (3)$$

The mean local volume fraction β of the oil at the position of the probe can be estimated from the conductance signal from either the front or the rear sensor. For the front sensor β is given by

$$\beta = \frac{1}{T} \sum_{i=1}^{N} (t_{2f,i} - t_{1f,i}) \qquad (4)$$

2.2 The oil-water flow facility

The experiments described in this paper were carried out in the 80mm internal diameter, 2.5m long, vertical, perspex working section of a purpose built oil-water flow loop (figure 2). The dual-sensor probe described above was mounted in this working section at

a distance of approximately 1.5m from the entry point of the oil and water (see also section 3).

The oil and water were stored in a 2.5m^3 stainless steel separator tank. The water outlet was located close to the base of the tank, the oil outlet was selected using one of three manual valves, dependent upon the position of the oil-water interface. On leaving the tank the oil and water were conveyed through separate flow lines prior to being mixed together in a manifold just upstream of the working section. The oil and water flow lines each contained; (i) a pump capable of pumping up to about $20\,\text{m}^3\text{hr}^{-1}$ of liquid at 3 bar gauge pressure, (ii) an electro-pneumatic control valve and (iii) a turbine flow meter. For each flow line the liquid flow rate was controlled using a separate Proportional-Integral-Derivative controller so that the oil and water flow rates into the flow loop working section could be individually controlled, for long periods of time, to better than 0.5% of set-point flow rate. On emerging from the flow loop working section the oil-water mixture was piped back to the inlet of the separator tank in the form of a 'primary dispersion'. Gravity induced separation of the oil and water in the tank was accelerated with the aid of a coalescer cartridge which spanned the cross section of the separator tank. The oil used in the experiments described in this paper was Shellsol D70 with a density of $790\,\text{kgm}^{-3}$ and a kinematic viscosity of about $2\,\text{mm}^2\text{s}^{-1}$ at 20^{o}C.

At each flow condition investigated a reference measurement $\overline{\beta}_{ref}$ of the mean oil volume fraction in the working section was measured using a differential pressure technique, compensated for the effects of frictional pressure loss. This technique (figure 2) required a differential pressure transducer which was connected, via water filled lines, to two pressure tappings on the working section, separated by a vertical distance h equal to 1m. With reference to [11] $\overline{\beta}_{ref}$ is given by

$$\overline{\beta}_{ref} = \frac{\Delta p + F}{(\rho_w - \rho_o) g h} \qquad (5)$$

where Δp is the measured differential pressure, ρ_w is the water density, ρ_o is the oil density, g is the acceleration of gravity and F is a frictional pressure loss term which, with reference to [11], is given by

$$F = \frac{2\rho_w h f U_h^2}{D} \qquad (6)$$

where U_h is the homogeneous velocity (also known as the mixture superficial velocity), D is the internal diameter of the working section and f is a single phase friction factor (in the present investigation a value for f equal to 0.007 was used).

3. Experimental Results

A series of experiments was undertaken to measure the local oil volume fraction distribution and the local oil axial velocity distribution in the 80mm internal diameter working section of the flow loop described in section 2. Experiments were carried out for

values of water superficial velocity U_{ws} in the range $0.276\,\mathrm{ms}^{-1}$ to $0.417\,\mathrm{ms}^{-1}$ and for values of oil superficial velocity U_{os} in the range $0.025\,\mathrm{ms}^{-1}$ to $0.083\,\mathrm{ms}^{-1}$. [These are flow rates that might be expected to be encountered in small, older oil wells, producing oil at a few tens to a few hundred barrels per day and also producing significant quantities of water]. For the experiments described herein $\overline{\beta}_{ref}$ was in the range 0.047 to 0.205. For all of the experiments undertaken the flow regime was 'bubbly oil-in-water' with the oil droplets having an oblate spheroidal shape with the major axis, normal to the direction of motion, approximately 7mm long and the minor axis approximately 6mm long [12].

The dual-sensor probe described in section 2 was mounted in the flow loop working section, using a fully automated two-axis traversing mechanism, with the tip of the probe at a distance of approximately 1.5m from the inlet to the working section. At each flow condition the probe was traversed along eight equispaced radii with measurements being made at eight equispaced radial locations along each radius. The first radial position was the pipe centre whilst the last radial position was when the probe centerline was at a distance of 2mm from the pipe wall. At each measurement position signals from the two conductance sensors were obtained for a period of 120 seconds and the local axial oil velocity u_o and the local oil volume fraction β were calculated using equations 3 and 4 respectively. Convergence tests showed that the use of sampling periods greater than 120 seconds did not significantly alter the values of u_o and β obtained in this way. Diagrams showing u_o versus r/D and β versus r/D (where r represents radial probe position and D represents the pipe diameter) are given in figures 3 to 8 (the solid and dotted lines shown in these figures are simply lines connecting adjacent data points). It should be noted that for a given flow condition, the value of u_o or β at a given value of $|r/D|$ in figures 3 to 8 is actually an *averaged* value taken from measurements obtained at the same value of $|r/D|$ for each of the eight radii mentioned above. For reasons described extensively in a previous paper [2] measurements of u_o taken very close to the pipe wall using a dual-sensor probe *can* be unreliable. Consequently, these 'wall measurements' of u_o have been excluded from the graphs shown in figures 3 to 5.

From figures 3 to 5 it is clear that the local axial oil velocity distributions for all of the flow conditions investigated are 'power law' in shape [2] i.e. the profiles are of the form $u_o = u_{o,\max}(1-r/R)^p$ where $u_{o,\max}$ is the maximum value of the local oil velocity (at the pipe centre), R is the pipe radius and p is an exponent. However, from figures 6 to 8 it is apparent that the shape of the local oil volume fraction distribution varies significantly with the mean oil volume fraction $\overline{\beta}_{ref}$. For values of $\overline{\beta}_{ref}$ less than about 0.08, the local oil volume fraction distribution is approximately 'power law' in shape. For the middle values of $\overline{\beta}_{ref}$ investigated, i.e. for $\overline{\beta}_{ref}$ in the approximate range 0.08 to 0.15, the local oil volume fraction distribution is essentially flat, except toward the pipe wall. For higher values of $\overline{\beta}_{ref}$, i.e. greater than about 0.15, the local oil volume fraction distribution has a shape referred to in [13] as 'intermediate peaked'.

The shapes of the distributions of u_o versus r/D and β versus r/D will be discussed extensively in subsequent sections of this paper.

4. Comparison of Oil Droplet and Air Bubble Velocity Profiles

In section 3 it was stated that the oil velocity distribution for each of the flow conditions investigated was 'power law' in shape and of the form $u_o = u_{o,\max}(1-r/R)^p$. The exponent p can be used to characterise the shape of power law profiles because relatively low values of p indicate a relatively flat profile whilst relatively higher values of p indicate a profile with a relatively pronounced peak at the pipe centre [2]. Using curve fitting techniques the value of p was calculated for each of the oil-water flow conditions investigated in the present study. Figure 9 shows p plotted against $\overline{\beta}_{ref}$ for the oil-water data (diamonds). Also shown in figure 9 are values of the exponent p for velocity profiles of air bubbles in a bubbly-air-water flow (crosses). [NB: in figure 9, when considering the values of p relevant to air-water flows, the horizontal axis is taken to represent the mean air volume fraction $\overline{\alpha}$]. The air-water data shown in figure 9 (and represented by crosses) was taken by the authors of the present paper at similar flow conditions to those at which the oil-water data was taken (the air-water experiments are described in detail in [2]). Thus, the air-water data was taken using a dual-sensor conductance probe at an axial distance of 2m from the inlet of a vertical, 80mm internal diameter pipe. The mean air bubble diameter was about 5mm, the water superficial velocity was in the range $0.1\,\mathrm{ms}^{-1}$ to $1.15\,\mathrm{ms}^{-1}$ and the gas superficial velocity took values such that the mean gas volume fraction was in the range $0.01 < \overline{\alpha} < 0.08$, thus ensuring that the air-water flow regime was always bubbly. Inspection of figure 9 shows that the values of p for the oil velocity profiles are quite similar to the values of p for the air velocity profiles. In fact, the mean value of p for the oil data is 0.133 whilst for the air data it is 0.173. For values of dispersed phase volume fraction of about 0.05 to 0.06, where there are several data points for both the air-water and the oil-water experiments, the values of the exponent p are often very similar, indicating that the velocity profiles for the oil droplets and for the air bubbles are very similar in shape. This result is particularly noteworthy given that the oil droplets have a density which is about 630 times greater than the air bubbles.

Also shown in figure 9 in the form of a solid line is a correlation by van der Welle [3] expressing the exponent p as a function of $\overline{\alpha}$ for air-water flows. Although the van der Welle correlation was based on data taken in a vertical 100mm internal diameter pipe, and is really only valid for values of gas volume fraction greater than about 0.28, there is still remarkable agreement with the values of p obtained for the oil velocity profiles in the present study.

5. Comparison of Oil Droplet and Air Bubble Volume Fraction Profiles

Quantitative comparison of oil volume fraction profiles with air volume fraction profiles in vertical, bubbly, water continuous flows at similar flow conditions is really only feasible when the local volume fraction distribution of the dispersed phase is power law in shape. For other profile shapes (e.g. 'wall peaked' [13]) comparison of the oil and air

volume fraction profiles tends to be a qualitative rather than quantitative exercise. In the present investigation power law shaped oil volume fraction distributions were only observed for values of $\overline{\beta}_{ref}$ less than about 0.08 (see section 3). In the literature, although for air-water bubbly flows the local air volume fraction distribution can take a variety of shapes [13], for flows where the air bubble size is about 5mm or greater the air volume fraction profile is generally power law in shape. In the remainder of this section discussion is limited to such power law profiles.

For the oil-water experiments described in this paper for which $\overline{\beta}_{ref} < 0.08$ the local oil volume fraction distribution was of the form $\beta = \beta_{\max}(1 - r/R)^q$, where $\beta_{\max}$ is the maximum value of the local oil volume fraction which occurs at the pipe centre. In figure 10 the exponent q is shown plotted against $\overline{\beta}_{ref}$ for five distinct flow conditions. Also shown in figure 10 (dark line) is a plot of the Lucas et al [2] correlation $q = 0.9014e^{-4.823\overline{\alpha}}$, where $\overline{\alpha}$ represents mean air volume fraction, which was obtained by the authors of the current paper for air-water bubbly flows at similar flow conditions [2] (see also section 4). [NB: again, in figure 10, when considering air-water data, the horizontal axis must be assumed to represent $\overline{\alpha}$]. A further correlation relating q to $\overline{\alpha}$, obtained by van der Welle [3] for air-water flows is also shown in figure 10 (light line). It is apparent that the values of q for the oil-water data are somewhat lower than the values of q for the air-water data observed by Lucas et al [2], indicating that the oil volume fraction profiles are flatter than the air volume fraction profiles. However, the values of q for the oil-water data are scattered about the van der Welle correlation for q obtained for air-water data. Again, given the large density contrast between air and oil, the similarities in the shapes of the local dispersed phase volume fraction distributions as indicated by figure 10 are very noteworthy.

6. The Zuber-Findlay Distribution Parameter C_0

For many two phase flows (both vertical and inclined) the mean velocity $\overline{u}_d$ of the dispersed phase can be obtained from a relationship of the form

$$\overline{u}_d = C_0 U_h + u_{t0}(1 - \overline{\alpha}_d)^n \qquad (7)$$

where u_{t0} is the velocity of a single particle of the dispersed phase rising through the static continuous phase, n is an exponent, U_h is the homogeneous velocity (or mixture superficial velocity) , $\overline{\alpha}_d$ is the mean volume fraction of the dispersed phase and C_0 is the so called Zuber-Findlay distribution parameter [4]. The terms n and u_{t0} in equation 7 can be obtained from calculation or experiment whilst, under a given set of flow conditions, U_h and $\overline{\alpha}_d$ can often be obtained by measurement [11]. Consequently, if the relevant value of C_0 is known, equation 7 can be used to determine the mean dispersed phase velocity $\overline{u}_d$ (note that for vertical oil-in-water Lucas and Jin [14] found that

appropriate values for the terms n and u_{t0} are 2 and $0.167\,\mathrm{ms}^{-1}$ respectively). With reference to [4] the parameter C_0 is given by the expression

$$C_0 = \frac{\overline{\alpha_l j_l}}{\overline{\alpha}_d U_h} \qquad (8)$$

where α_l is the local dispersed phase volume fraction, j_l is the local homogeneous velocity and the overbar in the numerator of equation 8 represents averaging in the flow cross section. For the oil-water experiments described in section 3 of this paper the simplifying assumption was made that the local homogeneous velocity can be calculated using the relationship $j_l = (1-\beta)(u_o - u_{slip}) + \beta u_o$ where u_{slip} is the slip velocity between the oil and the water, which was set equal $0.167\,\mathrm{ms}^{-1}$. C_0 can then be calculated from the experimental data according to equation 8.

For the oil-water experiments carried out in the present investigation calculated values of C_0 are shown plotted against the mean oil volume fraction $\overline{\beta}_{ref}$ in figure 11. Also shown in figure 11 are calculated values of C_0 plotted against the mean air volume fraction $\overline{\alpha}$ for the air-water data taken by the authors of this paper at similar flow conditions [2] and described in sections 4 and 5 of this paper. It is clear from figure 11 that, for similar values of the mean dispersed phase volume fraction, the values of C_0 for the oil-water data (diamonds) are very similar to the values of C_0 for the air-water data (crosses). It is also apparent that the trend for C_0 to decrease towards unity with increasing air volume fraction, observed in bubbly air-in-water flows (for values of $\overline{\alpha}$ up to about 0.08), is continued for bubbly oil-in-water flows (for values of $\overline{\beta}_{ref}$ up to about 0.205). The mean value of C_0 for the air-water data shown in figure 11 is 1.084. The mean value of C_0 for the oil-water data is 1.035, which is also remarkably similar to the C_0 value of 1.036 observed by Lucas and Jin [14] for vertical, bubbly oil-in-water flows in a 150mm diameter pipe with a 42.86mm diameter centrebody. This suggests that, for vertical, bubbly oil-in-water flows, the distribution parameter C_0 may be remarkably insensitive to the pipe diameter and geometry.

7. Modelling the Local Oil Volume Fraction Distributions

In an attempt to explain the different shapes of the oil volume fraction profiles in a circular pipe by the use of mathematical modelling, the following oil droplet conservation equation, in cylindrical polar co-ordinates, was used

$$\frac{1}{r}\frac{\partial}{\partial r} r\beta u_r + \frac{1}{r}\frac{\partial}{\partial \theta}\beta u_\theta + \frac{\partial}{\partial z}\beta u_z = 0 \qquad (9)$$

where u_z, u_θ and u_r represent the local oil droplet velocities in the axial, azimuthal and radial directions respectively and where β is the local oil volume fraction. [NB: equation 9 is equivalent to stating that the divergence of the oil droplet flux is equal to zero i.e. $\nabla \cdot (\beta \mathbf{u}) = 0$]. By making the assumptions that the local oil volume fraction profile is (i) axisymmetric and (ii) fully developed in the axial direction, equation 9 can be simplified to give

$$\frac{d}{dr}(r\beta u_r) = 0 \qquad (10)$$

In equation 10, βu_r represents the local oil droplet flux per unit area normal to the radial direction. In the present study it was initially assumed from the work of Beyerlein [15] that this radial flux comprises two components. The first component is a diffusive flux arising from the local droplet diffusivity ε. The second component is due to a circulation induced, local hydrodynamic force [15] acting on the oil droplets which arises from the velocity profile of the continuous water phase. This hydrodynamic force gives rise to a local oil droplet velocity u_{hy} in the positive radial direction which is described in [15] and also discussed in more detail later in this section. Equation 10 can now be rewritten as

$$\frac{d}{dr} r\left\{\beta u_{hy} - \varepsilon \frac{d\beta}{dr}\right\} = 0 \qquad (11)$$

Integrating equation 11 gives

$$r\left\{\beta u_{hy} - \varepsilon \frac{d\beta}{dr}\right\} = K_0 \qquad (12)$$

where K_0 is a constant of integration. In equation 12 the quantity $(\beta u_{hy} - \varepsilon \frac{d\beta}{dr})$ represents the local *net* flux per unit area, normal to the radial direction, at a given point in the flow. At any given axial location in the pipe (away from the pipe inlet and the pipe outlet) there are no sources or sinks of oil droplets at the pipe centre or the pipe wall and so $(\beta u_{hy} - \varepsilon \frac{d\beta}{dr})$ must always be equal to zero. Thus K_0 must also be equal to zero. Equation 12 may now be manipulated to give

$$\frac{d\beta}{dr} = \frac{\beta u_{hy}}{\varepsilon} \qquad (13)$$

By considering the lateral forces on a solid sphere in a continuous liquid with shear, Beyerlein et al [15] reported that the local radial velocity u_{hy} imparted to spherical

droplets of the dispersed phase in a bubbly two phase flow, as a result of the velocity profile of the continuous liquid phase, is given by

$$u_{hy} = -c_1 \frac{du_L}{dr} \qquad (14)$$

where u_L is the local axial liquid velocity and where c_1 is positive, and constant for a given set of flow conditions. In the present study the local axial water velocity u_w may be approximated by the expression

$$u_w = u_o - u_{t0} \qquad (15)$$

where u_o is the local axial oil droplet velocity and u_{t0} is the terminal rise velocity of a single oil droplet in stationary water. It was shown in section 4 that the local axial oil velocity is of the form

$$u_o = u_{o,\max}(1 - r/R)^p \qquad (16)$$

By combining equations 14, 15 and 16 it can be shown that the local radial velocity u_{hy} imparted to the oil droplets as a result of shear in the water phase is given by

$$u_{hy} = K_{hy}(1 - r/R)^{p-1} \qquad (17)$$

where K_{hy} is positive and constant for a given set of flow conditions and where p is the exponent defined in section 4. Inspection of equation 17 shows that according to Beyerlein et al [15] the local radial velocity u_{hy} is always in the direction of increasing r.

With reference to work reported in [15] and [16] the local droplet diffusivity ε in the present investigation was assumed to have a maximum value at the pipe centre and to decay towards the pipe wall. The following expression for ε was adopted

$$\varepsilon = \frac{K_\varepsilon}{r}(1 - r/R)^{1-q} \qquad (18)$$

where K_ε is constant for a given set of flow conditions and where q is the exponent defined in section 5.

By combining equations 17, 18 and 13 the following expression relating the local oil volume fraction β to radial pipe position r was obtained.

$$\frac{d\beta}{dr} = \beta r \frac{K_{hy}}{K_\varepsilon}(1 - r/R)^{p+q-2} \qquad (19)$$

Equation 19 can be used to model the local oil volume fraction distribution in a so-called 'free stream' region of the flow. However, as briefly reported in [15] a 'bubble sub-layer' exists in which the local dispersed phase volume fraction decreases to zero toward the pipe wall. From the experimental data taken in the present study it was assumed that the bubble sub-layer existed in the region for which $|r/D| > 0.405$ and it was further assumed that in this sub-layer the value of β decreased linearly from its free stream value to zero at $|r/D| = 0.5$.

At a given flow condition equation 19 can be solved numerically to determine the free stream local volume fraction distribution provided (i) that β is known at one value of r (the initial condition) and (ii) that the appropriate value for the quantity K_{hy}/K_{ε} is known. At a given flow condition equation 19 was used to simulate the experimentally observed distribution of β with r by using the measured value of the local oil volume fraction at the pipe centre as the initial condition and by adjusting the value of K_{hy}/K_{ε} to give the best fit with the experimental data. The main purpose of this approach was to determine both the magnitude and sign of the quantity K_{hy}/K_{ε} at each of the flow conditions investigated. A value of $p = 0.133$ was used in equation 19, corresponding to the mean value for this variable for all of the oil-water flow conditions investigated in the present study (see section 4). A value of $q = 0.538$ was used in equation 19, this value corresponding to the mean value of q for those flow conditions in which the local oil volume fraction distribution was 'power law' in shape (see section 5). It should be noted however that the results predicted by equation 19 were not particularly sensitive to the precise value of q.

7.1 Application of the model to $\overline{\beta}_{ref} > 0.15$

In figures12a and 12b plots are shown of the experimentally observed local oil volume fraction distributions at two flow conditions for which these distributions have 'intermediate peaked' shapes, i.e. $\overline{\beta}_{ref} > 0.15$ (the exact flow conditions are given in the legend to figure 12). Also shown in figures 12a and 12b are the simulated local oil volume fraction distributions obtained using equation 19 in conjunction with the concept of the bubble sub-layer, as described above. For the flow condition where $\overline{\beta}_{ref} = 0.187$, the value of the quantity K_{hy}/K_{ε} which gave the best agreement with the experimental data was +70 (see Table I). For the flow condition for which $\overline{\beta}_{ref} = 0.205$ the appropriate value for K_{hy}/K_{ε} was +60. It can be seen from figures 12a and 12b that there is very good agreement between the experimentally observed and the simulated local oil volume fraction distributions.

7.2 Application of the model to $\overline{\beta}_{ref} < 0.08$

For the flow conditions at which the local oil volume fraction distributions were 'power law' in shape, i.e. $\overline{\beta}_{ref} < 0.08$, it was not possible to obtain agreement between the experimentally observed and simulated local oil volume fraction distributions unless *negative* values of K_{hy} / K_{ε} were used (Table I). This result indicates that the modelling approach suggested by Beyerlein [15], which proposed a shear induced hydrodynamic force on the droplets in the positive radial direction, is insufficient to explain all of the observed experimental results. However, by using the appropriate values of K_{hy} / K_{ε} from Table I, good agreement between the experimental and simulated distributions is obtained (figures 13a and 13b).

7.3 Application of the model to $0.08 \le \overline{\beta}_{ref} \le 0.15$

For $0.08 \le \overline{\beta}_{ref} \le 0.15$ simulated and experimentally observed local oil volume fraction distributions are shown in figures 14a and 14b. It can be seen from Table I that when $\overline{\beta}_{ref} = 0.135$ then K_{hy} / K_{ε} is equal to zero, suggesting that the net radial hydrodynamic force on each droplet is also zero and that the shape of the local oil volume fraction profile is purely due to the effects of diffusion.

7.4 Magnitude and direction of the net hydrodynamic force on the oil droplets

The values of K_{hy} / K_{ε} required to successfully simulate the experimentally observed local volume fraction distributions are shown in Table I for six different values of $\overline{\beta}_{ref}$. For $\overline{\beta}_{ref} < 0.08$ negative values of K_{hy} / K_{ε} are required and so it must be concluded that for such values of $\overline{\beta}_{ref}$ the resultant hydrodynamic force on the droplets is in the direction of the pipe centre. Also for $\overline{\beta}_{ref} < 0.08$ the magnitude of the quantity K_{hy} / K_{ε} is significantly greater ($\ge 520 m^{-2}$) than the magnitude of this quantity for $\overline{\beta}_{ref} > 0.15$ ($\le 70 m^{-2}$). This strongly suggests that the net hydrodynamic force on the droplets towards the pipe centre for $\overline{\beta}_{ref} < 0.08$ is significantly greater than the net hydrodynamic force on the droplets toward the pipe wall for $\overline{\beta}_{ref} > 0.15$

It should be noted that when K_{hy} / K_{ε} is negative it is implicit that the variation of the radial velocity of the oil droplets with r due to hydrodynamic effects will be of the form shown in equation 17 - except with a change of sign. Since the exact nature of this net inward hydrodynamic force on the oil droplets is unknown, the actual variation of the resultant radially inward droplet velocity with r is also unknown.

8. Radial Forces on Dispersed Phase Particles

In this section a qualitative discussion is given on possible sources of the radial hydrodynamic forces on particles of the dispersed phase in co-current, upward, bubbly two phase flows where the superficial velocity of the continuous phase is greater than zero. For very low dispersed phase volume fraction flows in which the dispersed particles

are relatively large compared to the pipe diameter [13], as was the case for the 6mm to 7mm oil droplets in the present investigation, it is widely reported in the literature [13] that the particles will tend to migrate toward the pipe centre, which may represent an equilibrium position for dispersed phase particles in very low volume fraction flows. Once the oil droplets are established at the pipe centre as described above, the low pressure region in their wakes will draw additional oil droplets towards the pipe centre as the oil volume fraction is increased. This may explain the observed tendency for the oil droplets to accumulate at the pipe centre for values of $\overline{\beta}_{ref}$ less than about 0.08, giving rise to power law shaped profiles.

As the oil volume fraction is increased further, the effects of droplet diffusion cause the oil droplets to migrate to those parts of the flow cross section where there is significant shear in the continuous phase velocity profile. Here, circulation induced forces (see section 7, [13] and [15]) give rise to radial droplet velocities in the direction of the pipe wall as described by equation 17. This in turn gives rise to the observed 'intermediate peaked' oil volume fraction profiles. [Note that the modelling work in section 7 suggests that the net hydrodynamic force moving each droplet toward the pipe centre, for $\overline{\beta}_{ref}$ less than about 0.08, is significantly greater than the net hydrodynamic force moving each droplet toward the pipe wall for $\overline{\beta}_{ref}$ greater than about 0.15].

For air-water flows there is a much greater tendency for the air bubbles to agglomerate into larger structures at the pipe centre (such as cap shaped bubbles) rather than to migrate away from the pipe centre. This is the probable reason why power law shaped profiles are observed for wide ranges of values of gas volume fraction in flows where gas is injected in the form of relatively large bubbles ($\geq 5\text{mm}$) [13]. In low volume fraction air-water flows in which the gas bubbles are relatively small (between 0.8mm to 3.6mm) there is a reduced tendency for the migration of bubbles into the wakes of other bubbles at the pipe centre [13] due to the relatively lower wake size of lower Reynolds number bubbles [17]. This could explain why for gas-liquid bubbly flows, in which the bubble size is in the range 0.8mm to 3.6mm, 'intermediate peaked' and 'wall peaked' gas volume fraction distributions are frequently observed [13].

9. Conclusions

A series of experiments was carried out on vertical, bubbly oil-in-water flows in an 80mm internal diameter pipe for values of water superficial velocity in the range $0.276\,\text{ms}^{-1}$ to $0.417\,\text{ms}^{-1}$, for values of oil superficial velocity in the range $0.025\,\text{ms}^{-1}$ to $0.083\,\text{ms}^{-1}$ and for values of the mean oil volume fraction $\overline{\beta}_{ref}$ in the range 0.047 to 0.205. The oil droplets were about 6mm to 7mm in size. For all of the flow conditions investigated, it was found that the velocity profile of the oil droplets was 'power law' in shape, with the peak velocity at the pipe centre and with the velocity declining to zero at the pipe wall. The shapes of the observed oil velocity distributions were very similar to the shapes of air velocity distributions obtained in bubbly air-water flows at similar flow conditions and with 5mm air bubbles. Values of the Zuber-Findlay distribution parameter C_0 for the oil-water flows were very similar to values of C_0 obtained for bubbly air-water flows at similar flow conditions. These results are noteworthy given the large density contrast between oil and air.

The shape of the local oil volume fraction distribution for the oil-in-water flows investigated was found to be dependent upon $\overline{\beta}_{ref}$. For values of $\overline{\beta}_{ref}$ less than about 0.08 the net hydrodynamic force on the oil droplets is relatively strong and acts in the direction of the pipe centre giving rise to local oil volume fraction distributions that are 'power law' in shape.

For values of $\overline{\beta}_{ref}$ in the range 0.08 to 0.15 the net hydrodynamic force on the droplets is close to zero with the resultant oil volume fraction distributions being mainly due to droplet diffusion and hence being essentially flat, apart from within the so-called bubble sub-layer adjacent to the wall.

For values of $\overline{\beta}_{ref}$ greater than about 0.15 the net hydrodynamic force on each droplet is relatively weak and in the direction of the pipe wall, giving rise to local oil volume fraction distributions with an 'intermediate peak' shape.

References

[1] Lucas G P, Wang M, Mishra R, Dai Y and Panayotopoulos N, Quantitative comparison of gas velocity and volume fraction profiles obtained from a dual-plane ERT system with profiles obtained from a local dual-sensor conductance probe, in a bubbly gas-liquid flow. 3rd International Symposium on Process Tomography in Poland, Lodz (2004).

[2] Lucas G P, Mishra R and Panayotopoulos N, Power law approximations to gas volume fraction and velocity profiles in low void fraction vertical gas-liquid flows, Flow Measurement and Instrumentation **15,** (2004) 271-283.

[3] van der Welle R, Void fraction, bubble velocity and bubble size in two phase flow, Int. J. Multiphase Flow. **11** (1985) 317-345.

[4] Zuber N and Findlay J A, Average volumetric concentration in two phase flow systems, ASME J. Heat Transfer **87** (1965) 453-468.

[5] Vigneaux P, Chenais P and Hulin J P, Liquid-liquid flows in an inclined pipe. AIChE Journal, Vol.34, No.5, (1988), 781-789.

[6] Farrar B and Bruun H H, A computer based hot-film technique used for flow measurements in a vertical kerosene-water pipe flow. Int. J. Multiphase Flow. **22** (4), (1996), 733-751.

[7] Hamad F A, Pierscionek B K and Bruun H H, A dual optical probe for volume fraction, drop velocity and drop size measurements in liquid-liquid two-phase flow. Meas. Sci. Technol. **11** (2000) 1307-1318.

[8] Zhao D, Guo L, Hu X, Zhang X and Wang X, Experimental study on local characteristics of il-water dispersed flow in a vertical pipe. Int. J. Multiphase Flow. **32** (10-11), (2006), 1254-1268.

[9] Lum J Y L, Al-Wahibi T and Angeli P, Upward and downward inclination oil-water flows. Int. J. Multiphase Flow. **32** (2006), 413-435.

[10] Wang M, Ma Y, Holliday N, Dai Y, Williams A and Lucas G, A High Performance EIT System, IEEE Sensors Journal **5** (No.2), (2005) 289-299.

[11] Lucas G P and Jin N D, Measurement of the homogeneous velocity of inclined oil-in-water flows using a resistance cross correlation flow meter, Meas. Sci. Technol. **12** (2001) 1529-1537.

[12] Mishra R, Lucas G P and Keickhoefer H, A model for obtaining the velocity vectors of spherical droplets in multiphase flows from measurements using an orthogonal four-sensor probe, Meas. Sci. Technol. **13** (2002), 1488-1498.

[13] Hibiki T and Ishii M, Distribution parameter and drift velocity of drift-flux model in bubbly flow, Int. J. Heat and Mass Transfer, **5**, (2001), 707-721.

[14] Lucas G P and Jin N D, Investigation of a drift velocity model for predicting superficial velocities of oil and water in inclined oil-in-water pipe flows with a centre body, Meas. Sci. Technol. **12** (2001) 1546-1554.

[15] Beyerlein S W, Cossmann R K and Richter H J, Prediction of bubble concentration profiles in vertical turbulent two-phase flow. Int. J. Multiphase Flow, **11**, Issue 5, (1985), 629-641.

[16] Lucas G P, Modelling velocity profiles in inclined multiphase flows to provide *a priori* information for flow imaging The Chemical Engineering Journal **56** (1995) 167-173.

[17] Brennen C E, fundamentals of multiphase flow, (2005) Cambridge University Press.

Figure Headings

Figure 1: The dual-sensor probe

Figure 2: Schematic of the 80mm i.d. flow loop working section

Figure 3: Local oil droplet axial velocity u_o versus r/D for values of mean oil volume fraction less than 0.08. [Squares :- $U_{ws} = 0.276\text{ms}^{-1}$, $U_{os} = 0.027\text{ms}^{-1}$. Diamonds:- $U_{ws} = 0.417\text{ms}^{-1}$, $U_{os} = 0.041\text{ms}^{-1}$].

Figure 4: Local oil droplet axial velocity u_o versus r/D for values of mean oil volume fraction between 0.08 and 0.15. [Squares :- $U_{ws} = 0.276\text{ms}^{-1}$, $U_{os} = 0.055\text{ms}^{-1}$. Diamonds:- $U_{ws} = 0.415\text{ms}^{-1}$, $U_{os} = 0.082\text{ms}^{-1}$].

Figure 5: Local oil droplet axial velocity u_o versus r/D for values of mean oil volume fraction greater than 0.15. [Squares :- $U_{ws} = 0.276\text{ms}^{-1}$, $U_{os} = 0.083\text{ms}^{-1}$. Diamonds:- $U_{ws} = 0.416\text{ms}^{-1}$, $U_{os} = 0.124\text{ms}^{-1}$].

Figure 6: Local oil volume fraction β versus r/D for values of mean oil volume fraction less than 0.08. [Squares :- $U_{ws} = 0.276\text{ms}^{-1}$, $U_{os} = 0.027\text{ms}^{-1}$. Diamonds:- $U_{ws} = 0.417\text{ms}^{-1}$, $U_{os} = 0.041\text{ms}^{-1}$].

Figure 7: Local oil volume fraction β versus r/D for values of mean oil volume fraction between 0.08 and 0.15. [Squares :- $U_{ws} = 0.276\text{ms}^{-1}$, $U_{os} = 0.055\text{ms}^{-1}$. Diamonds:- $U_{ws} = 0.415\text{ms}^{-1}$, $U_{os} = 0.082\text{ms}^{-1}$].

Figure 8: Local oil volume fraction β versus r/D for values of mean oil volume fraction greater than 0.15. [Squares :- $U_{ws} = 0.276\text{ms}^{-1}$, $U_{os} = 0.083\text{ms}^{-1}$. Diamonds:- $U_{ws} = 0.416\text{ms}^{-1}$, $U_{os} = 0.124\text{ms}^{-1}$].

Figure 9: Exponent p versus mean dispersed phase volume fraction for oil-water and air-water bubbly flows.

Figure 10: Exponent q versus mean dispersed phase volume fraction for oil-water and air-water bubbly flows.

Figure 11: Zuber-Findlay distribution parameter C_0 versus mean dispersed phase volume fraction for oil-water air-water flows. [The dotted line shows the trend of the air-water data. The solid line shows the trend of the oil-water data].

Figure 12: Simulated and experimental local oil volume fraction profiles for values of mean oil volume fraction greater than 0.15. [12(a):- $U_{ws} = 0.276\text{ms}^{-1}$, $U_{os} = 0.083\text{ms}^{-1}$. 12(b):- $U_{ws} = 0.416\text{ms}^{-1}$, $U_{os} = 0.124\text{ms}^{-1}$].

Figure 13: Simulated and experimental local oil volume fraction profiles for values of mean oil volume fraction less than 0.08. [13(a) :- $U_{ws} = 0.276\text{ms}^{-1}$, $U_{os} = 0.027\text{ms}^{-1}$. 13(b):- $U_{ws} = 0.417\text{ms}^{-1}$, $U_{os} = 0.041\text{ms}^{-1}$].

Figure 14: Simulated and experimental local oil volume fraction profiles for values of mean oil volume fraction between 0.08 and 0.15. [14(a):- $U_{ws} = 0.276\text{ms}^{-1}$, $U_{os} = 0.055\text{ms}^{-1}$. 14(b):- $U_{ws} = 0.415\text{ms}^{-1}$, $U_{os} = 0.082\text{ms}^{-1}$].

Table Heading

Table 1: Calculated values of K_{hy}/K_{ε} for six different flow conditions and the corresponding values of the mean oil volume fraction $\overline{\beta}_{ref}$.

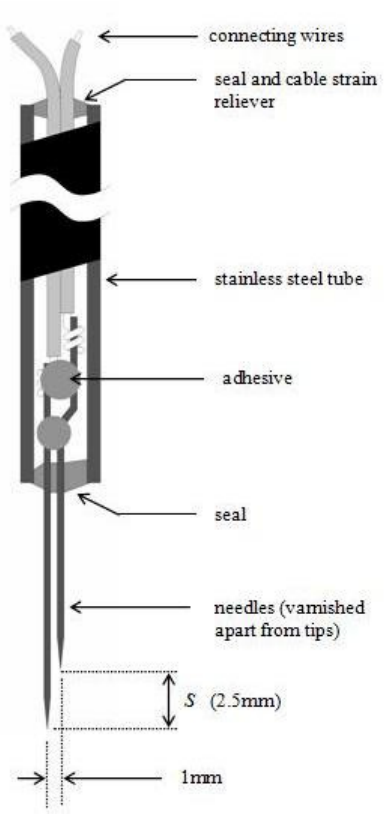
connecting wires
seal and cable strain reliever
stainless steel tube
adhesive
seal
needles (varnished apart from tips)
S (2.5mm)
1mm

Figure 1

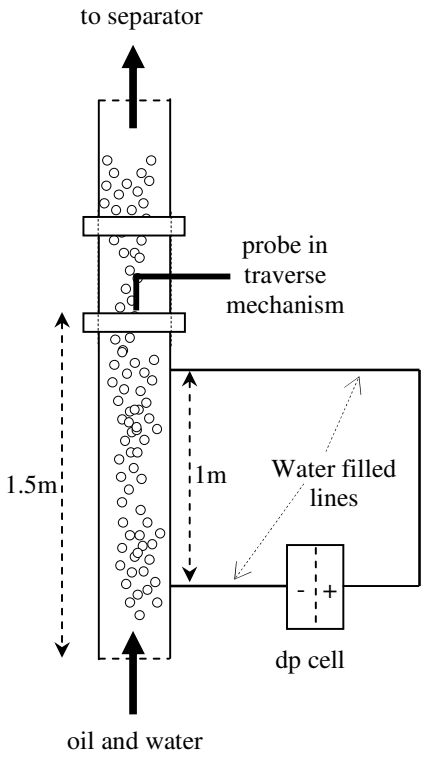
to separator
probe in
traverse
mechanism
1.5m
1m
Water filled
lines
-
+
dp cell
oil and water

Figure 2

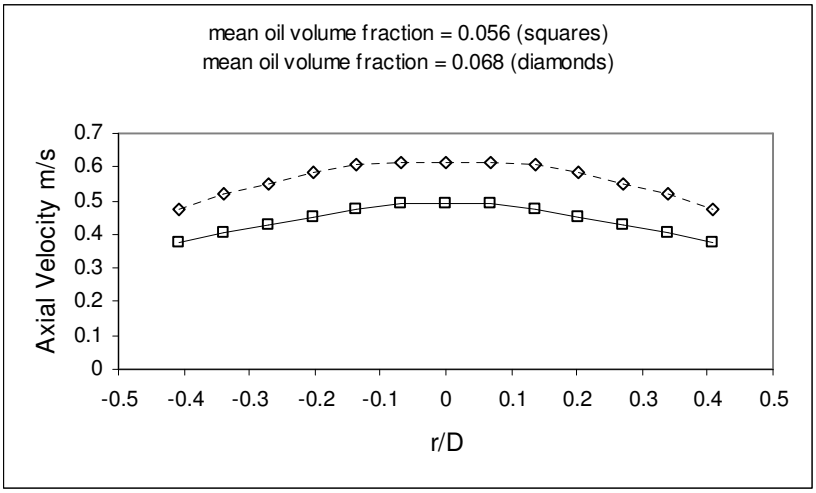
mean oil volume fraction = 0.056 (squares)
mean oil volume fraction = 0.068 (diamonds)
Axial Velocity m/s
0.7
0.6
0.5
0.4
0.3
0.2
0.1
0
-0.5
-0.4
-0.3
-0.2
-0.1
0
0.1
0.2
0.3
0.4
0.5
r/D

Figure 3

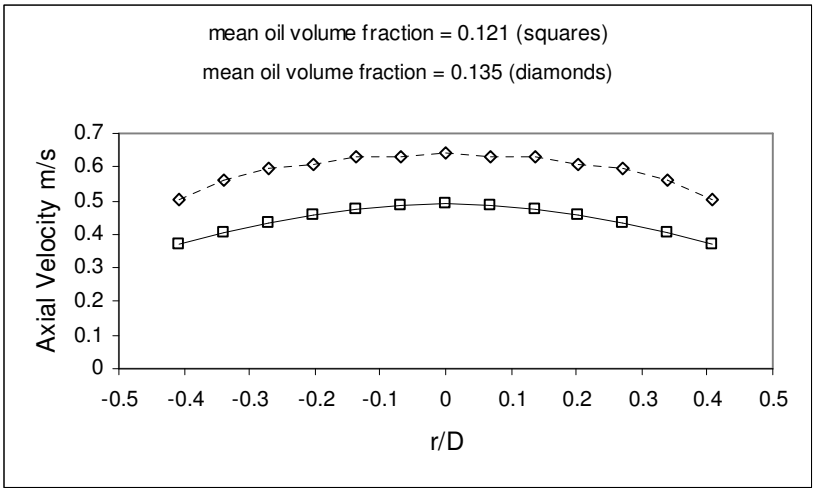
mean oil volume fraction = 0.121 (squares)
mean oil volume fraction = 0.135 (diamonds)
Axial Velocity m/s
0.7
0.6
0.5
0.4
0.3
0.2
0.1
0
-0.5
-0.4
-0.3
-0.2
-0.1
0
0.1
0.2
0.3
0.4
0.5
r/D

Figure 4

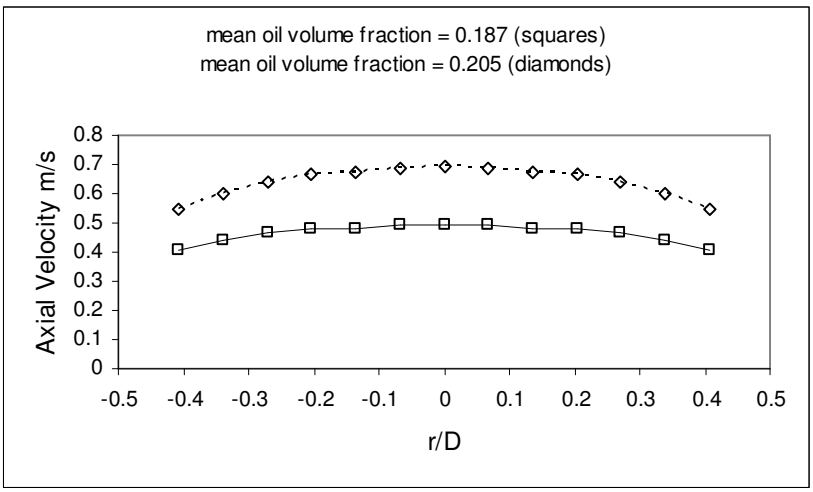
mean oil volume fraction = 0.187 (squares)
mean oil volume fraction = 0.205 (diamonds)
Axial Velocity m/s
0.8
0.7
0.6
0.5
0.4
0.3
0.2
0.1
0
-0.5
-0.4
-0.3
-0.2
-0.1
0
0.1
0.2
0.3
0.4
0.5
r/D

Figure 5

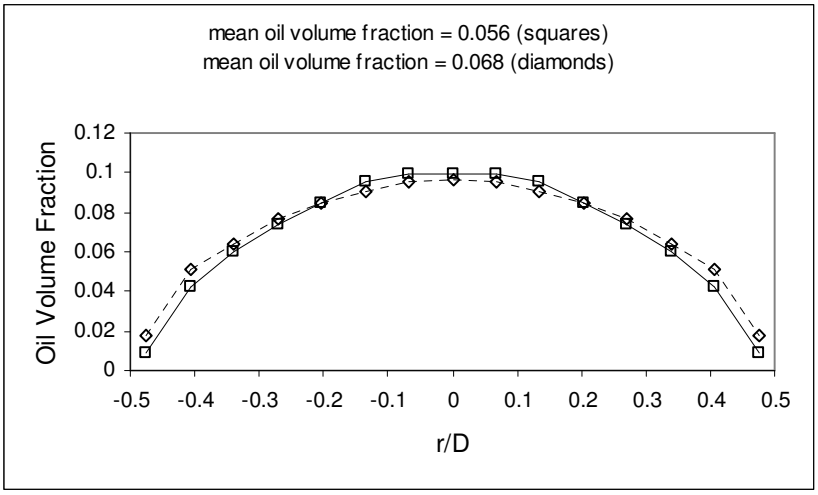
mean oil volume fraction = 0.056 (squares)
mean oil volume fraction = 0.068 (diamonds)
Oil Volume Fraction
0.12
0.1
0.08
0.06
0.04
0.02
0
-0.5
-0.4
-0.3
-0.2
-0.1
0
0.1
0.2
0.3
0.4
0.5
r/D

Figure 6

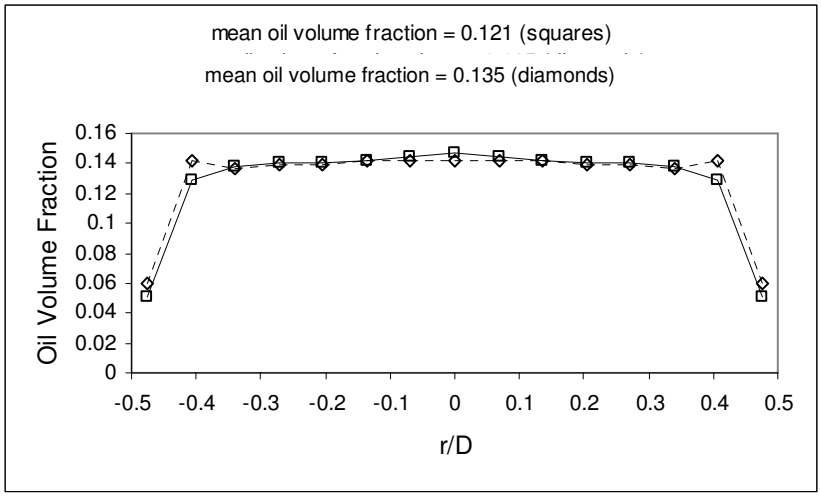
mean oil volume fraction = 0.121 (squares)
mean oil volume fraction = 0.135 (diamonds)
Oil Volume Fraction
0.16
0.14
0.12
0.1
0.08
0.06
0.04
0.02
0
-0.5
-0.4
-0.3
-0.2
-0.1
0
0.1
0.2
0.3
0.4
0.5
r/D

Figure 7

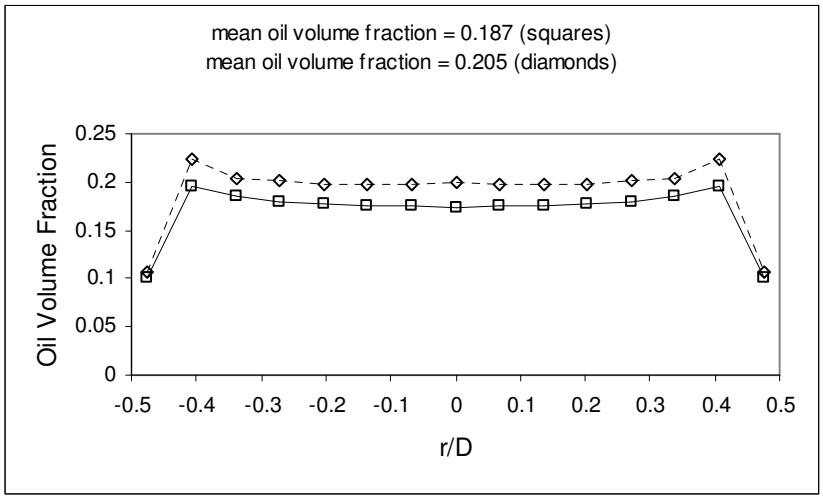
mean oil volume fraction = 0.187 (squares)
mean oil volume fraction = 0.205 (diamonds)
Oil Volume Fraction
0.25
0.2
0.15
0.1
0.05
0
-0.5
-0.4
-0.3
-0.2
-0.1
0
0.1
0.2
0.3
0.4
0.5
r/D

Figure 8

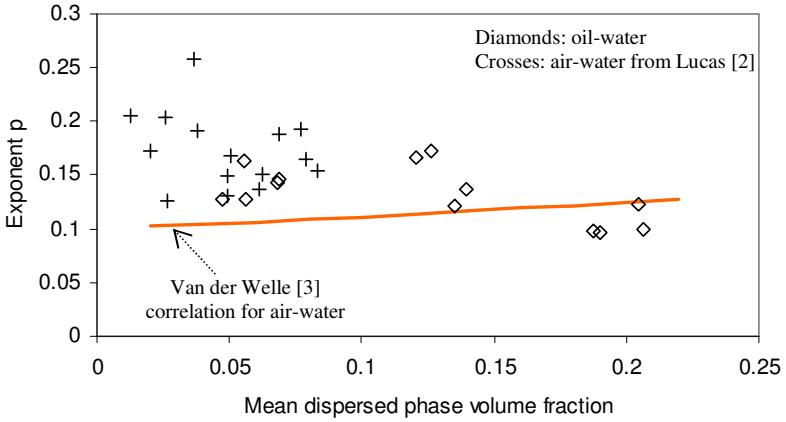
Diamonds: oil-water
Crosses: air-water from Lucas [2]
Van der Welle [3]
correlation for air-water
Exponent p
Mean dispersed phase volume fraction
0.3
0.25
0.2
0.15
0.1
0.05
0
0
0.05
0.1
0.15
0.2
0.25

Figure 9

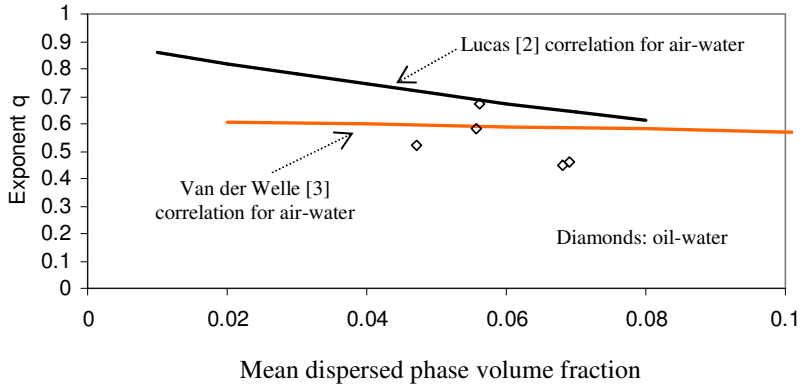
Exponent q
1
0.9
0.8
0.7
0.6
0.5
0.4
0.3
0.2
0.1
0
0
0.02
0.04
0.06
0.08
0.1
Lucas [2] correlation for air-water
Van der Welle [3]
correlation for air-water
Diamonds: oil-water
Mean dispersed phase volume fraction

Figure 10

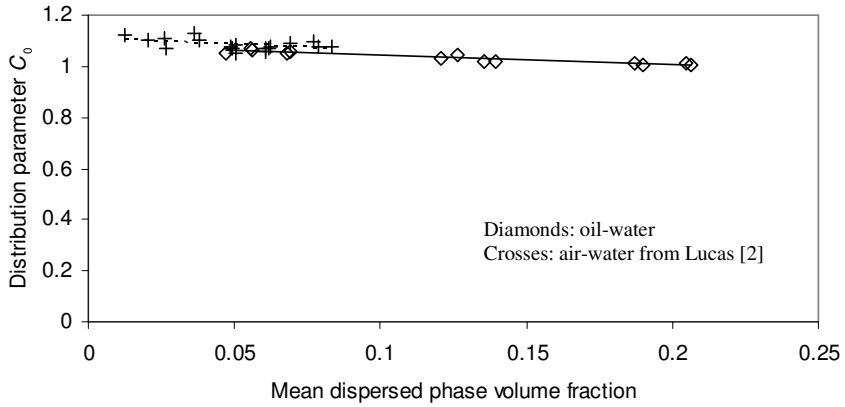
1.2
1
0.8
0.6
0.4
0.2
0
Distribution parameter C_0
0
0.05
0.1
0.15
0.2
0.25
Mean dispersed phase volume fraction
Diamonds: oil-water
Crosses: air-water from Lucas [2]

Figure 11

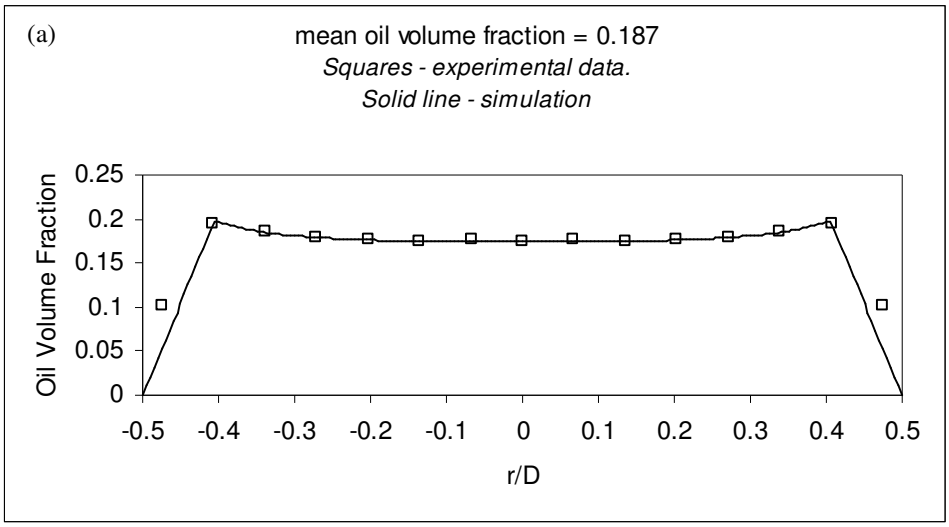
(a)
mean oil volume fraction = 0.187
Squares - experimental data.
Solid line - simulation
Oil Volume Fraction
0.25
0.2
0.15
0.1
0.05
0
-0.5
-0.4
-0.3
-0.2
-0.1
0
0.1
0.2
0.3
0.4
0.5
r/D

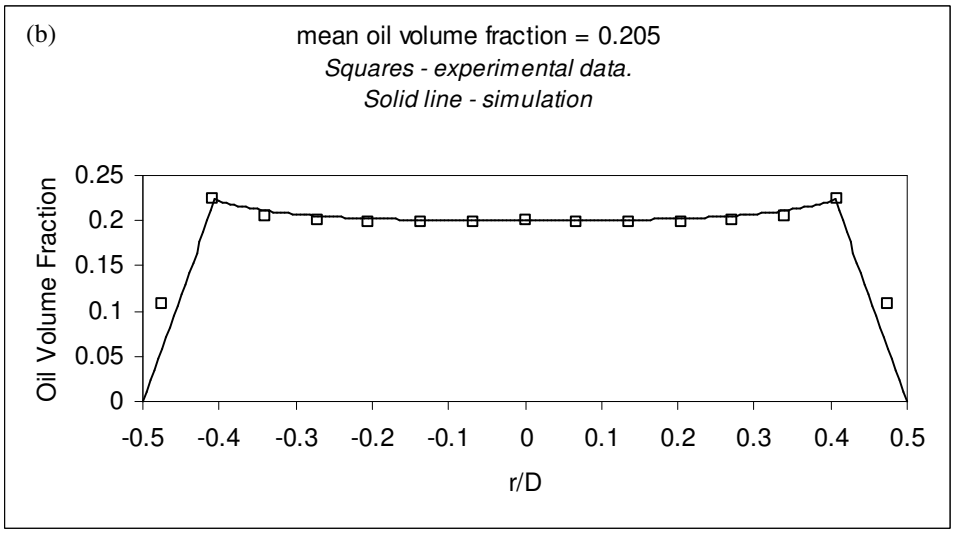
(b)
mean oil volume fraction = 0.205
Squares - experimental data.
Solid line - simulation
Oil Volume Fraction
0.25
0.2
0.15
0.1
0.05
0
-0.5
-0.4
-0.3
-0.2
-0.1
0
0.1
0.2
0.3
0.4
0.5
r/D

Figure 12

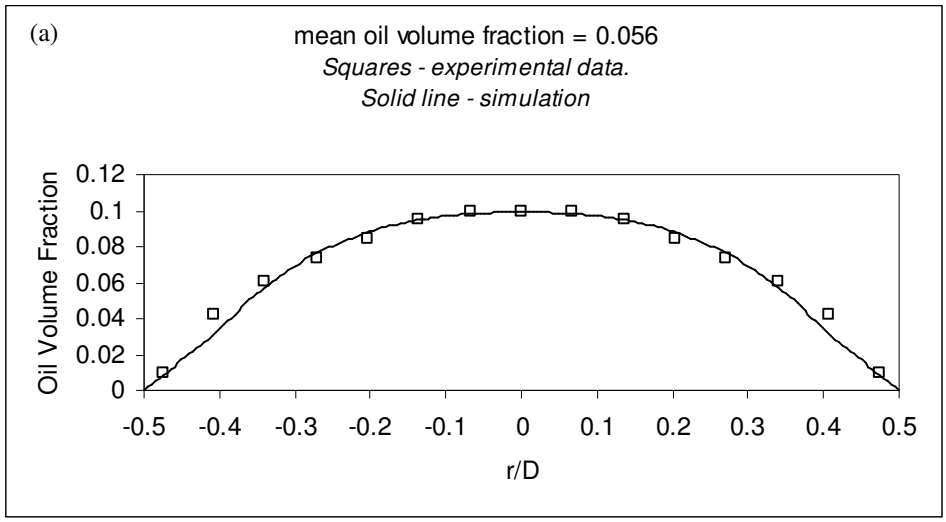
(a)
mean oil volume fraction = 0.056
Squares - experimental data.
Solid line - simulation
Oil Volume Fraction
0.12
0.1
0.08
0.06
0.04
0.02
0
-0.5 -0.4 -0.3 -0.2 -0.1 0 0.1 0.2 0.3 0.4 0.5
r/D

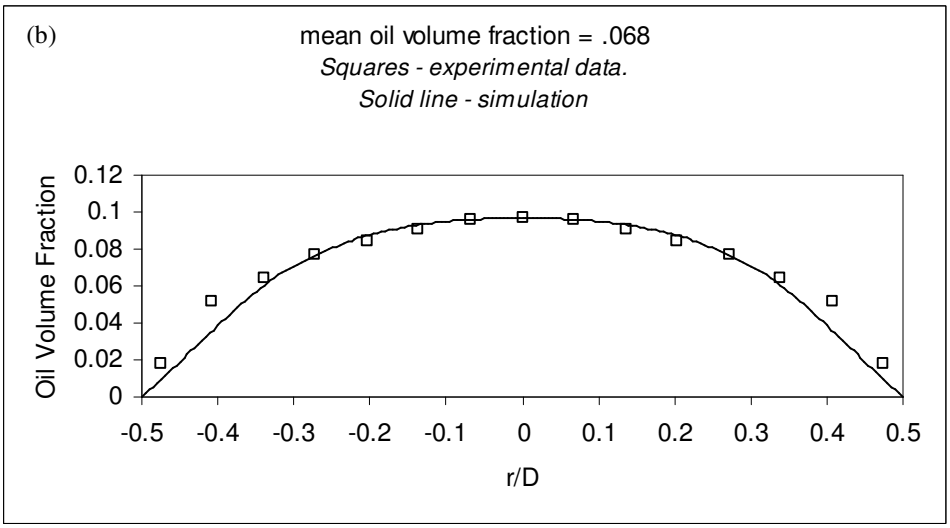
(b)
mean oil volume fraction = .068
Squares - experimental data.
Solid line - simulation
Oil Volume Fraction
0.12
0.1
0.08
0.06
0.04
0.02
0
-0.5 -0.4 -0.3 -0.2 -0.1 0 0.1 0.2 0.3 0.4 0.5
r/D

Figure 13

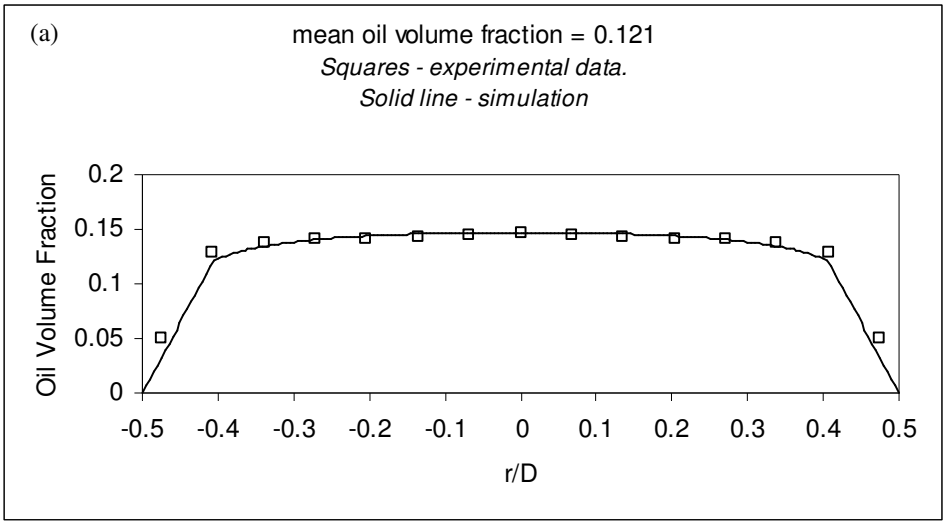
(a)
mean oil volume fraction = 0.121
Squares - experimental data.
Solid line - simulation
Oil Volume Fraction
0.2
0.15
0.1
0.05
0
-0.5
-0.4
-0.3
-0.2
-0.1
0
0.1
0.2
0.3
0.4
0.5
r/D

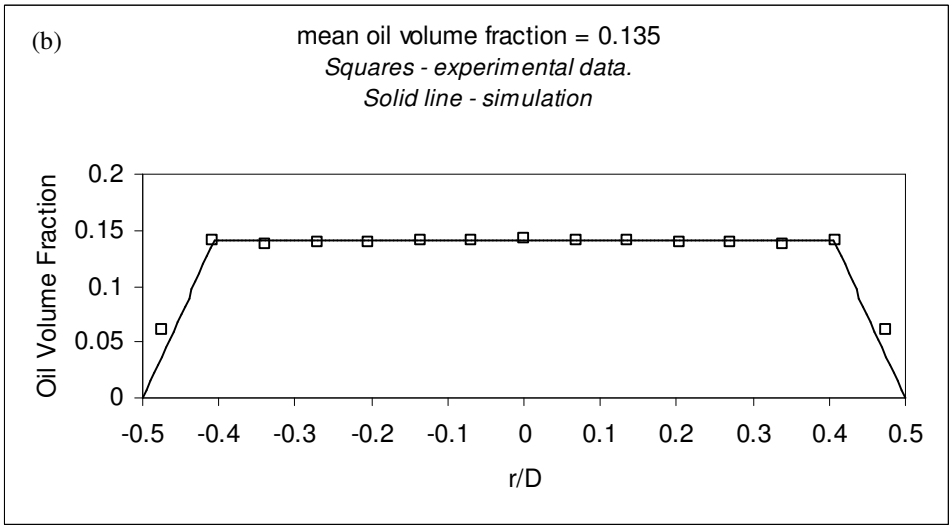
(b)
mean oil volume fraction = 0.135
Squares - experimental data.
Solid line - simulation
Oil Volume Fraction
0.2
0.15
0.1
0.05
0
-0.5
-0.4
-0.3
-0.2
-0.1
0
0.1
0.2
0.3
0.4
0.5
r/D

Figure 14

K_{hy} / K_{ε}	$\overline{\beta}_{ref}$
-600	0.056
-520	0.068
-100	0.121
0	0.135
+70	0.187
+60	0.205

Table 1